Is Cerocene Really a Ce(III) Compound? All-Electron Spin−Orbit Coupled CASPT2 Calculations on M(η^8-C_8H_8)$_2$ (M = Th, Pa, Ce)

Andrew Kerridge, Rosemary Coates, and Nikolas Kaltsoyannis*

Department of Chemistry, University College London, 20 Gordon Street, London WC1H 0AJ, U.K.

Received: September 2, 2008; Revised Manuscript Received: January 13, 2009

Spin−orbit free CASPT2 wave functions and energies are presented for the ground and 31 excited states of three f element sandwich molecules; thorocene ($ThCOT_2$), protactinocene ($PaCOT_2$), and cerocene ($CeCOT_2$). Ground-state metal-ring centroid distances are optimized at this level and show excellent agreement with experiment. The effects of spin−orbit coupling are included and are found to be negligible for the ground states of $ThCOT_2$ and $CeCOT_2$, for which comparison of the electronic excitation energies is made with experimental data. For $PaCOT_2$, spin−orbit coupling is found to alter significantly the energies and nature of the ground and low-lying excited states, and good agreement is obtained with previous computational data. The ground state of $CeCOT_2$ is found to be strongly multiconfigurational, though not in the same way as previously reported. The relationship of this result to previous computational and experimental data is discussed, as is the most appropriate way to view the electronic structure of $CeCOT_2$. It is concluded that the occupations of the natural orbitals produce a more reliable description of the $CeCOT_2$ ground state than does the configurational admixture.

1. Introduction

The lanthanocenes and actinocenes $MCOT_2$ (M = f element; COT = η^8-C_8H_8) are the prototypical f element organometallic compounds. The structurally characterized examples all feature planar and parallel carbocyclic rings,[1−3] sandwiching the metal center in an eclipsed (D_{8h}) orientation, a motif not found elsewhere in the periodic table. Superficially, it would appear that they have straightforward electronic structures. COT requires two electrons to become a 10π electron, Hückel aromatic ring, and hence the metal atom must relinquish four electrons, attaining a formal oxidation state of IV. Any remaining metal electrons are then accommodated in f-based orbitals.

The most intriguing, and controversial, of these systems is cerocene, $CeCOT_2$. Originally prepared in Italy and mischaracterized,[4] it was prepared deliberately by Streitwieser et al. who reported photoelectron spectroscopic and computational studies consistent with the tetravalent formulation.[5] Raymond also argued strongly, primarily on structural grounds, for such an ionic formulation of COT-based complexes of the lanthanides and actinides.[6,7] This interpretation of the bonding is troubling, however, as it implies the presence of two highly reducing COT^{2-} rings in close proximity to the strongly oxidizing Ce^{4+} cation. Such worries find ample support in the computational contributions of Dolg and co-workers, who reported the results of ab initio calculations on $CeCOT_2$ and its actinide analogue $ThCOT_2$.[8−12] They concluded that the ground state of $ThCOT_2$ is $^1A_{1g}$, and that the dominant configuration to this state is closed shell, with formally dianionic rings and no metal-localized electrons (i.e., Th(IV)). However, the dominant contribution (c. 80%) to the $^1A_{1g}$ ground state of $CeCOT_2$ is a configuration which can be considered to have a hole in the highest occupied ring-based π orbitals of e_{2u} symmetry, and a single metal-localized valence $4f_\delta$ electron. The two unpaired electrons are coupled antiferromagnetically, and the direct product of their spatial symmetries is A_{1g}. The analogue of the dominant configuration in $ThCOT_2$ contributes only ca. 20% to the ground-state wave function. Thus, $CeCOT_2$ is best described as a Ce(III) compound containing two COT rings each carrying a formal 1.5^- charge.

In 1996, Dolg et al.'s prediction was tested experimentally using *XANES*. The absorption K-edge of the cerium center in $CeCOT''_2$, $CeCOT'''_2$, $[CeCOT_2]^-$, and $[CeCOT''_2]^-$ (COT'' = η^8-1,4-$(TMS)_2C_8H_6$, COT''' = η^8-1,3,6-$(TMS)_3C_8H_5$) was found to lie in the trivalent rather than the tetravalent range, seemingly confirming the computational data.[13] Nearly a decade later, similar experiments on the parent $CeCOT_2$ came to the same conclusion.[14] Furthermore, Amberger has shown that optical spectroscopic properties of substituted cerocenes may be more consistent with a bonding model based on Ce(III) than Ce(IV).[15]

Notwithstanding this computational and experimental evidence, Streitwieser argued, on the basis of chemical and electrochemical studies, that it "it is still chemically reasonable and consistent to regard the central metal in this case as formally +4".[16] More recently, attention has turned to the pentalene (Pn, η^8-C_8H_6) analogue of $CeCOT_2$. Balazs et al., after detailed spectroscopic, magnetic and DFT studies, conclude that for $CePn_2$, "a classification of a formal oxidation state IV is recommended".[17] Interestingly, some of the same authors have also studied the permethylated analogue, $CePn^*_2$ (Pn* = η^8-C_8Me_6) using similar methodology, and concluded that "the [XANES spectroscopy] gives strong evidence for a formal valency close to Ce(III) in this molecule".[18] Clearly the debate continues.

$CeCOT_2$ and $CePn^*_2$ have both been described as examples of the self-contained Kondo effect in a single molecule.[14,18] Kondo systems are well-known and widely studied in solid-state physics and arise when a local magnetic moment spin polarizes local conduction electrons to form a magnetic singlet (see ref 19 and, e.g., refs 20 and 21). Kondo insulators are typically lanthanide-based, for example CeRhSb, YbB_{12}, and TmSe, and it is not implausible that the origins of Kondo states

10.1021/jp807804w CCC: $40.75
Published on Web 03/03/2009

in extended systems should contribute to unusual electronic structures in molecular compounds.

It is generally accepted that, as the actinide series is crossed, the chemistry becomes increasingly lanthanide-like, with the variable valency of the early actinide elements being replaced by a dominant trivalent oxidation state.[22] It might therefore be expected that, if $CeCOT_2$ does indeed have a multiconfigurational ground state, the ground states of the later actinocenes should increasingly resemble this, that is as the actinide series is crossed there should be an increasing degree of multiconfigurational character to the ground-state wave functions. Motivated by this expectation, we have embarked on a computational investigation of the actinocenes using a scalar relativistic variant of the complete active space self-consistent field (CASSCF) approach,[23−25] with additional corrections for (a) dynamic correlation (included perturbatively via complete active-space second-order perturbation theory (CASPT2)[26]), and (b) spin−orbit coupling.[27] In this contribution, we report the first results of this study and show that our methodology produces results for $ThCOT_2$ and $PaCOT_2$, which very much agree with previous experimental and computational data. By contrast, the same approach applied to $CeCOT_2$ yields a rather different picture from that previously reported.

2. Computational Details

Unless indicated otherwise, all calculations were performed using the *MOLCAS 6.4* code.[28] Spin−orbit free (SOF-) and spin−orbit coupled (SOC-)CASPT2 calculations were performed using all-electron ANO basis sets for all atoms and incorporating scalar relativistic effects via the second-order Douglas−Kroll Hamiltonian.[25] The basis sets used were as follows. For the metal atoms, correlation-consistent basis sets, constructed by Roos,[29] were employed, contracted as (27s24p18d14f)/[10s9p7d5f] for Th and Pa, and as (25s22p15d11f)/[9s8p5d4f] for Ce. These bases are of approximate VQZ quality. For C and H, ANO basis sets of DZP were used. This basis set combination, basis A, was used throughout, unless indicated otherwise.

We also performed a smaller number of calculations using two other basis combinations. Basis B retains the DZP bases for the ligand atoms, but includes g functions for the metal atoms, ((27s24p18d14f6g)/[10s9p7d5f3g] for Th and Pa, (25s22p15d11f4g)/[9s8p5d4f3g] for Ce). Basis C includes the larger metal bases and also improves the C and H functions to TZP. The results of these calculations are discussed in section 3.3 of the main text.

Reference orbitals for the CASSCF calculations were generated from restricted Hartree−Fock (RHF) calculations using the basis sets described above. In the case of $PaCOT_2$, an $S = {}^1/_2$ system, reference orbitals were obtained from RHF calculations performed on the cation. The improved-virtual-orbital (IVO) method[30] was used to generate more compact virtual orbitals than would be obtained from a standard RHF calculation.

In all calculations using the *MOLCAS* code, the COT ring was assumed to be planar and of D_{8h} symmetry, with $r_{CC} = 1.404$ Å and $r_{CH} = 1.087$ Å, as used in previous work.[9,10] This ring structure was held fixed during numerical optimization of the metal-COT ring centroid distance at the CASPT2 level.

Restrictions of *MOLCAS 6.4* require the calculations to be performed under D_{2h} symmetry. Bearing this in mind, we use the irreducible representations (irreps) of this point group in our discussions. This is necessary because in the subduction from D_{8h} to D_{2h} symmetry, certain formally orthogonal orbitals are allowed to mix. In terms of metal d and f levels, mixing of d_σ ($m_l = 0$) and d_δ ($m_l = \pm 2$), f_σ ($m_l = 0$) and f_δ ($m_l = \pm 2$), and f_π ($m_l = \pm 1$) and f_ϕ ($m_l = \pm 3$) can (in principle, at least) occur. Where relevant, we also use the irreps of D_{8h} to aid comparison with previous work. When this is the case, the representation in D_{8h} follows that in D_{2h}, and is enclosed in parentheses. We stress that the systems considered here have inversion symmetry, and so metal-based d- and f-levels span gerade and ungerade irreps, respectively.

All data presented in section 3 were obtained from state-averaged CASSCF calculations, where the state average is taken over the ground and first excited states of a given spatial and spin symmetry. As well as reducing the likelihood that the states obtained are local, rather than global, minima, averaged states lead to more reliable spin−orbit coupling results. Such results are known to be highly sensitive to state overlap,[31] which can be non-negligible in the absence of state averaging. It should be noted, however, that all discussion and analysis of natural orbitals and their occupations[32] uses the true natural orbitals for the state under consideration and not the pseudonatural orbitals derived from the state-averaged electron density (as are generated by default in *MOLCAS*).

The SOF-CASSCF calculated states were used as a basis for SOC calculations. These calculations were performed using the restricted active space state interaction (RASSI) formalism.[27] State energies were adapted according to the SOF-CASPT2 results. In the double point group D_{2h}^*, the direct product $\Gamma_{g,u} \times E_{1/2g} = E_{1/2g,u}$ for any irrep Γ of D_{2h}, and so for clarity we list the D_{2h} SOF states of which the SOC states are composed in our discussions.

The *Gaussian 03* code[33] was used to perform a vibrational analysis of $ThCOT_2$. For this calculation, the structure was optimized using density functional theory with the B3LYP hybrid exchange-correlation functional.[34−36] Dunning's cc-pVDZ basis set[37] was employed for C and H, and the small-core SDD effective core potential[38,39] with associated basis set was used for Th.

2.1. Active Spaces. We have performed calculations with two different active spaces. The first set of calculations was aimed at establishing the CASPT2 equilibrium metal-ring separations of the three target systems, for which we chose a larger active space incorporating sixteen orbitals. The orbitals used can be understood with reference to Figure 1, a qualitative molecular orbital energy level diagram for an early actinocene. Of the 16 orbitals, 6 were doubly occupied in the RHF-IVO reference calculations. This active space was used to ensure that the role of valence d levels in bonding was properly accounted for; in addition to the highest lying a_g and b_{1g} (e_{2g}), and a_u and b_{1u} (e_{2u}) ring-based occupied levels, whose inclusion in the active space is standard in previous work,[9−11,40,41] the lower lying b_{2g} and b_{3g} (e_{1g}) levels were included, ensuring that d_σ, d_δ, and f_δ electrons, which span these irreps, were all well correlated. We adopt the notation CASSCF(n, m) (or CASPT2(n, m)) to indicate the explicit correlation of n electrons in m orbitals, and so our $ThCOT_2$ and $CeCOT_2$ partial optimizations were conducted at the CASPT2(12,16) level. $PaCOT_2$, with one more valence electron, was optimized at the CASPT2(13,16) level. Table 1 defines the orbitals included in this active space in terms of the RHF-IVO reference orbitals.

Our second active space is smaller and was used to calculate the two lowest energy states of the two lowest multiplicities of each system for each of the eight irreps of the D_{2h} point group, at the optimized geometries obtained with the larger active spaces. The smaller active space differs from that shown in Table 1 in that the doubly occupied reference orbitals of b_{2g}

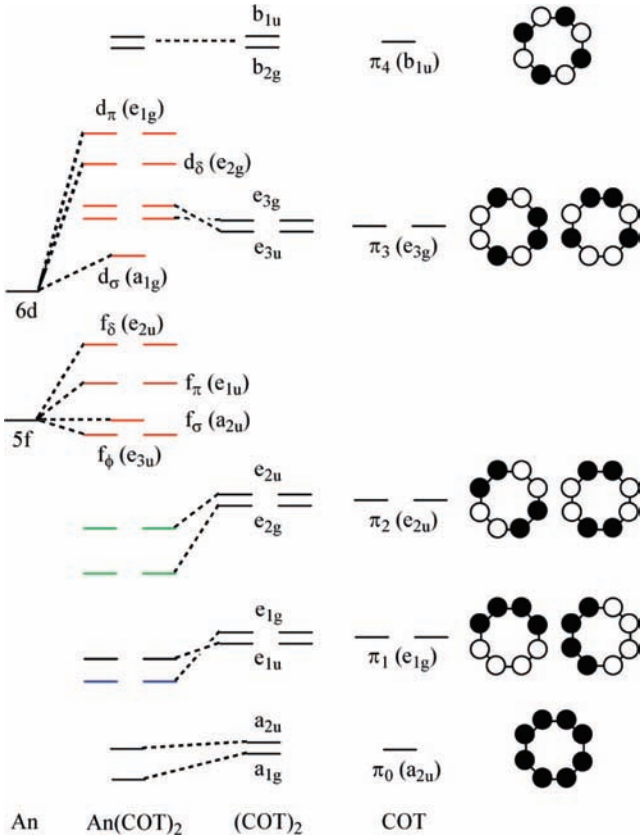

Figure 1. Qualitative molecular orbital energy level diagram for an early actinocene. Green levels are occupied ligand levels included in both active spaces used in this study. Blue levels are occupied ligand levels included only in the larger active space. Red levels are metal and unoccupied ligand levels that can be partially occupied in the active spaces.

TABLE 1: Active Space Orbitals Used in Optimizations of the Metal−Ring Centroid Distances, Expressed in Terms of the RHF-IVO Reference Orbitals

D_{2h} irrep	a_g	b_{1g}	b_{2g}	b_{3g}	a_u	b_{1u}	b_{2u}	b_{3u}
occupied	1	1	1	1	1	1	0	0
virtual	1	1	1	1	1	1	2	2

TABLE 2: Comparison of the Size of the Configuration Spaces Associated with the Active Spaces Used in This Study

active space orbitals	$ThCOT_2$	$PaCOT_2$	$CeCOT_2$
16	4 013 380	11 451 440	4 013 380
14	63 251	250 534	63 251

and b_{3g} (e_{1g}) symmetry are removed (Figure 1). Calculations reported here using this active space are therefore CASPT2(8,14) ($ThCOT_2$ and $CeCOT_2$) or CASPT2(9,14) ($PaCOT_2$). The smaller active space reduces the computational cost of calculations significantly, while excluding from the configuration space only configurations corresponding to excitations from deep lying ligand levels. This reduction is therefore expected to have minimal impact on the excited-state spectrum. Table 2 shows how the reduction in active space size alters the size of the configuration space.

3. Results

3.1. Spin−Orbit Coupling Free Calculations. ***(a) $ThCOT_2$.*** Previous work[10] indicates that $ThCOT_2$ has a ^1A_g ($^1A_{1g}$) ground state, and our SOF-CASPT2(12,16) calculations confirm this assignment. Numerical optimization of the COT centroid−Th separation for this state yields a minimum energy at 2.015 ± 0.001 Å, in excellent agreement with the experimentally determined separation of 2.004 Å.[2] We then performed state-averaged SOF-CASPT2(8,14) calculations at the optimized geometry to identify the relative energy, orbital, and multiconfigurational character of the two lowest energy singlet and triplet states of each irrep of the D_{2h} point group (32 states in total). Table 3 shows the relative energy and dominant orbital characteristics of the lowest energy states of each irrep and spin multiplicity.

TABLE 3: For $ThCOT_2$, the Relative SOF-CASPT2(8,14) Energies, and Orbital Character, of the Lowest Energy Singlet and Triplet States of Each D_{2h} Irrep[a]

state	ΔE (eV)	dominant character	state	ΔE (eV)	dominant character
^1A_g	0	d^0f^0	^1A_u	2.47	d^1_σ
$^1B_{1g}$	3.97	d^1_σ	$^1B_{1u}$	2.47	d^1_σ
$^1B_{2g}$	4.40	covalent (f_ϕ)	$^1B_{2u}$	4.91	covalent (f_ϕ)
$^1B_{3g}$	4.40	covalent (f_ϕ)	$^1B_{3u}$	4.91	covalent (f_ϕ)
^3A_g	3.66	d^1_σ	^3A_u	2.49	d^1_σ
$^3B_{1g}$	3.66	d^1_σ	$^3B_{1u}$	2.49	d^1_σ
$^3B_{2g}$	3.68	covalent (f_ϕ)	$^3B_{2u}$	4.48	covalent (f_ϕ)
$^3B_{3g}$	3.68	covalent (f_ϕ)	$^3B_{3u}$	4.48	covalent (f_ϕ)

[a] When the dominant character is described as covalent, this indicates strong mixing between metal and ligand levels. Because only excitations from a_g and b_{1g} (e_{2g}) and a_u and b_{1u} (e_{2u}) ligand-based orbitals are allowed, ligand configurations can be inferred from the metal occupancy and state parity.

The ^1A_g ($^1A_{1g}$) ground state is dominated (90.1%) by the expected closed-shell Th(IV) d^0f^0 configuration, with the remainder of the wave function being distributed over a large number of configurations. This is a reflection of the flexibility of these calculations and *not* an indication of significant multiconfigurational character. The ground-state natural orbital occupancies (NOOs)[32] of the active space orbitals, shown in Figure 2 and in Table 4, support this assertion. NOOs can be considered an indicator of multiconfigurational character; NOOs deviating from integer values >0.1 signify a strongly multiconfigurational system.[42]

Clearly the ground state of $ThCOT_2$ is not strongly multiconfigurational. As can be seen in Table 4, the vast majority (97.75%) of the active space density occupies orbitals closely resembling those that were doubly occupied in the RHF-IVO reference wave function. The largest occupations of the weakly occupied orbitals occur in the b_{2g} and b_{3g} (e_{1g}/e_{3g}), and b_{2u} and b_{3u} (e_{1u}/e_{3u}) orbitals (0.037 and 0.043 respectively). These orbitals are ligand-based, involving little occupation of metal levels. The weakly occupied a_u and b_{1g} levels, with occupation numbers of ≤0.01, correspond to metal f_δ and d_δ levels respectively.

Figure 3 illustrates the relative energies of all 32 states calculated here and also indicates their multiconfigurational character in terms of the weights of the configurations contributing to each state. The ground and first four excited states are all predominantly single configurational, and the principal configuration of the first four excited states is d_σ^1, essentially corresponding to an intramolecular charge transfer from the COT rings to the metal to create formally Th(III) states. Th(III) is a strongly reducing oxidation state, and there are very few trivalent compounds of Th. A rare example is $ThCp''_3$ ($Cp'' = C_5H_3(SiMe_3)_2$), which has been shown both experimentally[43] and computationally[44] to have a d_σ^1 ground-state configuration. This ties in well with the present calculations, which show that

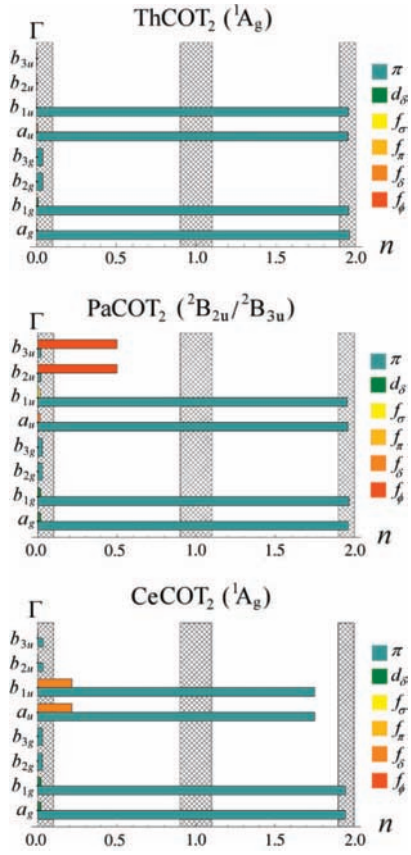

Figure 2. Natural orbital occupancies n of the 14 active space orbitals of the SOF ground states of the target systems. Bars terminating outside of the crosshatched areas indicate strong multiconfigurational character.

TABLE 4: Natural Occupation Numbers of the Active Space Orbitals in the CASPT2(8,14) ^{1}A$_g$ ThCOT$_2$ Ground State

symmetry	orbital character	occupation	symmetry	orbital character	occupation
a_g	π	1.960	a_u	π	1.951
	d_σ	0.001		f_δ	0.006
b_{1g}	π	1.957	b_{1u}	π	1.954
	d_δ	0.010		f_δ	0.000
b_{2g}	π	0.037	b_{2u}	covalent	0.001
				π	0.043
b_{3g}	π	0.037	b_{3u}	covalent	0.001
				π	0.043

occupation of the 6d$_\sigma$ level in the trivalent first excited states is energetically more favorable than any 5f occupation.

There is a clear relationship between excitation energy and metal level occupancy, and from this it can be deduced that there is a metal level energy ordering of $E(d_\sigma) < E(f_\sigma) < E(d_\delta)$. The spectrum also suggests that the ligand a_g and b_{1g} (e_{2g}) levels lie below the a_u and b_{1u} (e_{2u}) levels, with *ungerade* states involving d level occupation lying below their *gerade* counterparts. It would also appear that the f_ϕ level lies close in energy to the ligand b_{2u}/b_{3u} levels, resulting in strong mixing. It is important to remember that this description of the excited states in terms of the one-electron levels is only approximate, because i) the orbital character of the states shown in Figure 3 corresponds only to the dominant configuration, and ii) the CASSCF methodology allows orbital optimization in each state presented here.

Experimentally, "a broad band of low intensity...centered at 450 nm (= 2.76 eV) with a shoulder at shorter wavelength" is

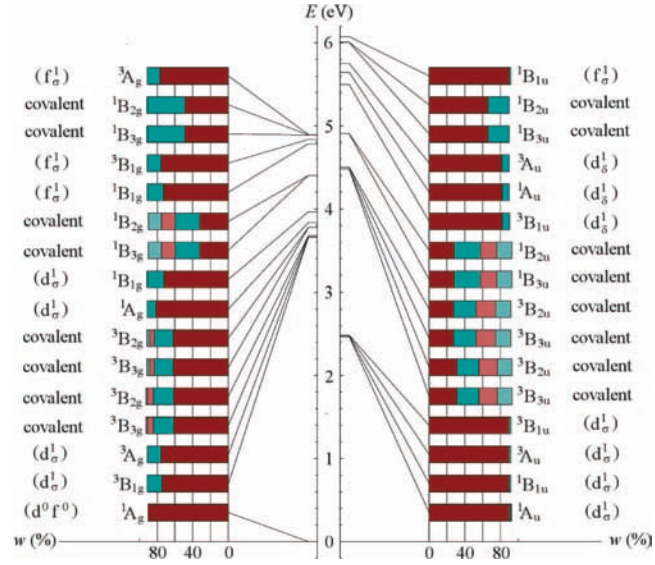

Figure 3. Relative energies and multiconfigurational character of the 32 ThCOT$_2$ SOF states considered in this study. Different colored blocks correspond to different configurations and are ordered in terms of decreasing weight (w). All configurations with weights greater than 1% are shown here. Dominant orbital characteristics are given in parentheses. Because only excitations from a_g and b_{1g} (e_{2g}) and a_u and b_{1u} (e_{2u}) ligand-based orbitals are allowed, ligand configurations can be inferred from the metal occupancy and state parity.

observed in the UV−vis spectrum of ThCOT$_2$.[45] The SCF-Xα method has been used[46] to assign this as a ligand to metal charge transfer transition, involving excitation into an f_ϕ level. The energy of this transition was calculated to be 3.03 eV. The corresponding states in our calculations (^{1}B$_{2u}$/^{1}B$_{3u}$, exhibiting strong ligand character) lie some 4.91 eV above the ground state, close to the value of 5.29 eV found in ref 10, and hence we suggest that the SCF-Xα assignment is incorrect. We find the lowest energy *ungerade* singlet state (^{1}B$_{1u}$) to lie 2.47 eV above the ground state. The energy of this state relative to the ground-state is not given in ref 10, but the energy of the equivalent triplet state is quoted as 2.54 eV (MCSCF) or 2.45 eV (MRCISD), in excellent agreement with our lowest ^{3}B$_{1u}$ state energy of 2.49 eV (Table 3).

Transition to the D_{2h} ^{1}B$_{1u}$ state is formally dipole-forbidden in D_{8h} symmetry. However, it seems likely that the experimentally observed band is indeed due to transitions to the *ungerade* states located at ca. 2.5 eV; the next ungerade states lie some 2 eV higher in energy. The purely electronic ring $\pi \rightarrow d_\sigma$ transitions will become weakly allowed through coupling to vibrational modes, which lower the point group of the system to D_{2h} (such couplings will also account for the broadness of the experimental peak). A frequency analysis of the ThCOT$_2$ ground state revealed several symmetry-lowering vibrational modes, of which two examples are given in Figure 4.

(b) PaCOT$_2$. SOF-CASPT2(13,16) optimization of the metal−ring centroid distance of the doubly degenerate ^{2}B$_{2u}$/^{2}B$_{3u}$ (E_{3u}) f_ϕ^1 ground-state yielded 1.969 ± 0.001 Å. There is no experimental value with which to compare this separation but a crude comparison can be made with the average of the experimental ThCOT$_2$ and UCOT$_2$ ring metal separations, 2.004 Å and 1.924 Å, respectively.[2] Our value is in excellent agreement with this average value of 1.964 Å, as well as with the 1.975 Å calculated previously by Li and Bursten[47] using DFT with the PW91[48] exchange-correlation functional.

State-averaged SOF-CASPT2(9,14) calculations were subsequently performed in order to characterize the two lowest

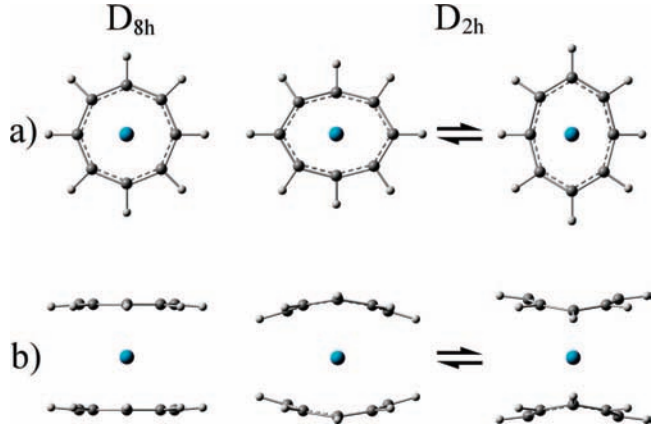

Figure 4. Two examples of calculated vibrational modes, which lower the symmetry of thorocene to D_{2h}. a) was calculated to occur at 377 cm^{-1}, and b) at 265 cm^{-1}.

TABLE 5: For $PaCOT_2$, the Relative SOF-CASPT2(9,14) Energies, and Orbital Character, of the Lowest Energy Doublet and Quartet States of Each D_{2h} Irrep[a]

state	ΔE (eV)	dominant character	state	ΔE (eV)	dominant character
^2A_g	0.59	d^1_σ	^2A_u	1.10	f^1_δ
$^2B_{1g}$	2.38	$d^1_\sigma f^1_\sigma$	$^2B_{1u}$	0.04	f^1_σ
$^2B_{2g}$	2.47	$d^1_\sigma f^1_\phi$	$^2B_{2u}$	0.00	f^1_ϕ
$^2B_{3g}$	2.47	$d^1_\sigma f^1_\phi$	$^2B_{3u}$	0.00	f^1_ϕ
^4A_g	2.27	$d^1_\sigma f^1_\sigma$	^4A_u	3.34	$f^1_\pi f^1_\phi$
$^4B_{1g}$	2.27	$d^1_\sigma f^1_\sigma$	$^4B_{1u}$	3.38	$f^1_\pi f^1_\phi$
$^4B_{2g}$	2.40	$d^1_\sigma f^1_\sigma$	$^4B_{2u}$	3.19	$f^1_\sigma f^1_\phi$
$^4B_{3g}$	2.40	$d^1_\sigma f^1_\sigma$	$^4B_{3u}$	3.19	$f^1_\sigma f^1_\phi$

[a] Because only excitations from a_g and b_{1g} (e_{2g}) and a_u and b_{1u} (e_{2u}) ligand-based orbitals are allowed, ligand configurations can be inferred from the metal occupancy and state parity.

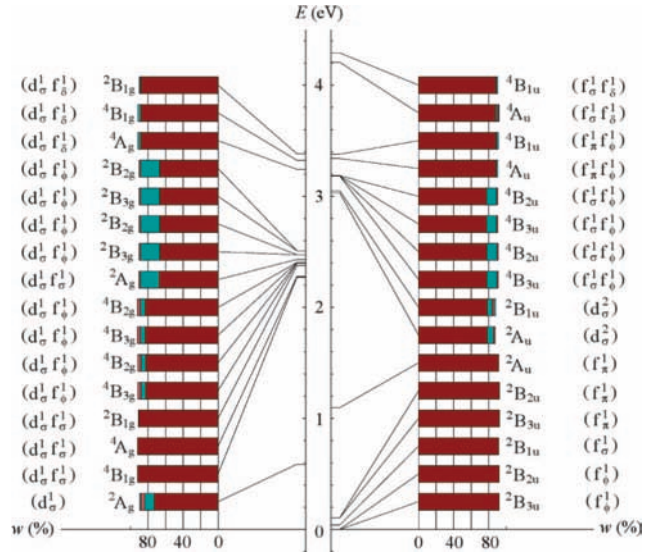

Figure 5. Relative energies and multiconfigurational character of the 32 $PaCOT_2$ SOF states considered in this study. Different colored blocks correspond to different configurations and are ordered in terms of decreasing weight (w). All configurations with weights greater than 1% are shown here. Dominant orbital characteristics are given in parentheses. Because only excitations from a_g and b_{1g} (e_{2g}) and a_u and b_{1u} (e_{2u}) ligand-based orbitals are allowed, ligand configurations can be inferred from the metal occupancy and state parity.

energy doublet and quartet states of each D_{2h} irrep, that is the $PaCOT_2$ analogues of the 32 states calculated for $ThCOT_2$. The $^2B_{2u}/^2B_{3u}$ ground state shows single-configuration character, as for $ThCOT_2$, and is dominated (92.0%) by occupation of the f_ϕ level. The $^2B_{1u}$ state, a single configuration state involving occupation of the f_σ level, lies just 0.04 eV above the ground state, with all other states lying significantly higher in energy. The lowest energy state of each irrep and spin-multiplicity is given in Table 5, and a summary of all states and their orbital and multiconfigurational character is given in Figure 5.

There is very little significant multiconfigurational character in the states calculated here, with all having a leading configuration comprising at least 66% (and typically much more) of the total wave function. It is worth emphasizing that all the states were obtained at the ground-state equilibrium geometry, and so the higher lying excited states may show multiconfigurational character because the molecular structure is nonoptimal.

The energy ordering of the metal levels is clear; $E(f_\phi) \sim E(f_\sigma) < E(f_\pi) < E(d_\sigma) \ll E(f_\delta)$. Typically, d^1f^1 excited-state occupation is preferred to f^2 occupation. This does not, however, unambiguously identify the relative positions of the a_g and b_{1g} (e_{2g}), and a_u and b_{1u} (e_{2u}) ligand levels, because strong f−f correlation also plays an important role in the relative energies of the states.

Examination of the ground-state NOOs in Figure 2 initially suggests that the $PaCOT_2$ ground state has strong multiconfigurational character, with ca. half-integer occupation of the b_{2u} and b_{3u} active-space orbitals. However, this is a symmetry artifact. In D_{8h}, the ground state is doubly degenerate, and so we present the NOOs averaged over the two contributing components; this is reflected in partial occupation of each f_ϕ level. In light of this, we conclude that the SOF ground state of $PaCOT_2$ does not show significant multiconfigurational character, in agreement with Figure 5.

Experimental UV−vis data are available only for $PaTMCOT_2$ (TMCOT = η^8-$C_8(CH_3)_8$) but have been used to estimate that an optically allowed transition in $PaCOT_2$ should occur at ca. 3.4 eV.[49] Previous work[47,50] has shown that the effects of spin−orbit coupling are pronounced in this system, and so we defer discussion of the nature of the optically accessible excited-state until section 3.2.

(c) $CeCOT_2$. As for $ThCOT_2$ and $PaCOT_2$, we began with larger active-space calculations of the equilibrium metal-ring separation of the $CeCOT_2$ ground state. SOF-CASPT2(12,16) calculations located a ^1A_g ground state, with a ring centroid−Ce separation of 1.964 ± 0.001 Å, in excellent agreement with the accepted (although unpublished) experimentally determined separation of 1.969 Å (ref 10). As with $ThCOT_2$, state-averaged SOF-CASPT2(8,14) calculations at the optimized geometry were then used to identify the relative energy, orbital, and multiconfigurational character of the two lowest energy singlet and triplet

TABLE 6: For $CeCOT_2$, the Relative SOF-CASPT2(8,14) Energies, and Orbital Character, of the Lowest Energy Singlet and Triplet States of Each D_{2h} Irrep[a]

state	ΔE (eV)	dominant character	state	ΔE (eV)	dominant character
^1A_g	0	d^0f^0	^1A_u	2.39	f^1_σ
$^1B_{1g}$	1.10	f^1_σ	$^1B_{1u}$	2.47	f^1_σ
$^1B_{2g}$	1.14	f^1_π	$^1B_{2u}$	2.47	f^1_π
$^1B_{3g}$	1.14	f^1_π	$^1B_{3u}$	2.47	f^1_π
^3A_g	1.10	f^1_σ	^3A_u	2.38	f^1_σ
$^3B_{1g}$	1.10	f^1_σ	$^3B_{1u}$	2.38	f^1_σ
$^3B_{2g}$	1.16	f^1_π	$^3B_{2u}$	2.46	f^1_π
$^3B_{3g}$	1.16	f^1_π	$^3B_{3u}$	2.46	f^1_π

[a] Because only excitations from a_g and b_{1g} (e_{2g}) and a_u and b_{1u} (e_{2u}) ligand-based orbitals are allowed, ligand configurations can be inferred from the metal occupancy and state parity.

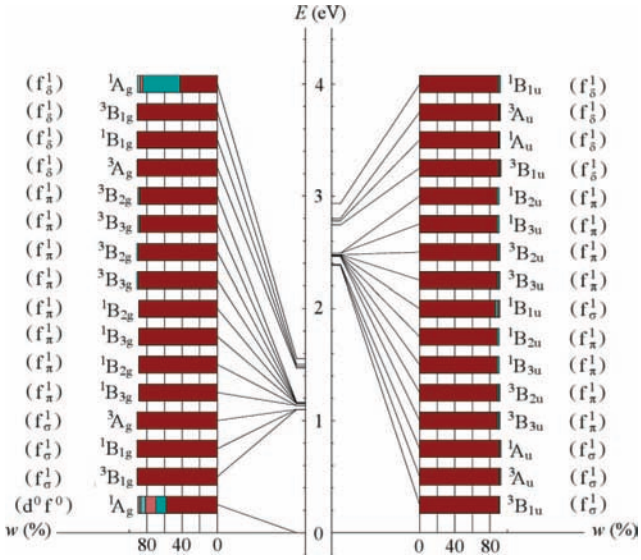

Figure 6. Relative energies and multiconfigurational character of the 32 $CeCOT_2$ SOF states considered in this study. Different colored blocks correspond to different configurations. All configurations with weights greater than 1% are shown here. Dominant orbital characteristics are given in parentheses. Because only excitations from a_g and b_{1g} (e_{2g}) and a_u and b_{1u} (e_{2u}) ligand-based orbitals are allowed, ligand configurations can be inferred from the metal occupancy and state parity.

states of each D_{2h} irrep. Table 6 collects the relative energies and dominant orbital characteristics of the lowest energy states of each irrep and spin-multiplicity, and a summary of all 32 states and their orbital and multiconfigurational character is given in Figure 6.

By contrast to Figures 3 and 5, the analogous data for the target actinocenes, Figure 6 indicates that the vast majority of the $CeCOT_2$ states are dominated by a single configuration. The exceptions are the two ^1A_g states, the compositions of which are shown in more detail in Figure 7. Both states appear to show pronounced multiconfigurational character but, as for the ground-state of $PaCOT_2$, that of the first excited ^1A_g state is due to symmetry requirements. The ground state, however, shows distinct multiconfigurational character, although the configurations making up this state are rather different from those previously reported by Dolg et al.[9,10] Whereas the previous calculations suggested a leading f^1 configuration, our two-state averaged calculation shows that almost 60% of the ground-state wave function consists of the "traditional" Ce(IV) d^0f^0 configuration. Only 23.4% of this state has an f^1 configuration, and we also calculate an 8.7% contribution from f^2 states. It is our

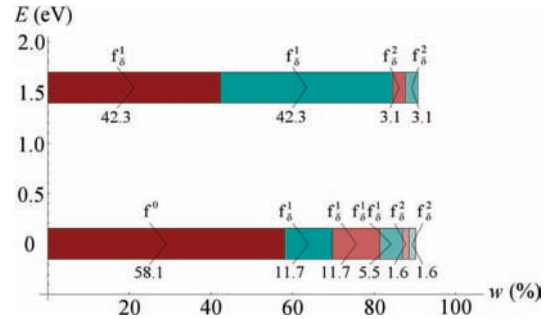

Figure 7. Contributing configurations to the ground and first excited ^1A_g states of $CeCOT_2$, obtained from a two state averaged calculation. As discussed in the main text, these contributions are highly sensitive to the number of states included in the average.

TABLE 7: Natural Occupation Numbers of the Active Space Orbitals in the CASPT2(8,14) ^1A_g $CeCOT_2$ Ground State

symmetry	orbital character	occupation	symmetry	orbital character	occupation
a_g	π	1.947	a_u	π	1.751
	d_δ	0.020		f_δ	0.216
b_{1g}	π	1.947	b_{1u}	π	1.751
	d_δ	0.020		f_δ	0.216
b_{2g}	π	0.030	b_{2u}	f_ϕ	0.001
				π	0.035
b_{3g}	π	0.030	b_{3u}	f_ϕ	0.001
				π	0.035

first excited ^1A_g state, c. 1.5 eV above the ground state, which has a dominant f^1 configuration.

The ground-state NOOs of the $CeCOT_2$ active space orbitals are given in Figure 2 and Table 7. Comparison with those of $ThCOT_2$ indicates a strong similarity between the two systems, with the exception of the a_u and b_{1u} (e_{2u}) ring π and f_δ levels. These orbitals are fully occupied and unoccupied respectively in the RHF-IVO calculations of both systems and essentially remain so following the CAS calculation on $ThCOT_2$. By contrast, they show a significant partial population in the active space calculation on $CeCOT_2$, with a ca. 0.25 reduction in population of the ring π-based levels accompanied by a similar enhancement of the f_δ orbital population. Whereas in $ThCOT_2$ the active space density is very similar to that of the uncorrelated RHF-IVO calculation (as noted in section 3.1(a), 97.75% occupies orbitals closely related to those of the RHF calculation), in $CeCOT_2$ only 92.45% of the density occupies equivalent orbitals.

Using the configurational admixture as a basis for evaluating the total f_δ occupation n_f, and making the assumption that the $CeCOT_2$ a_u and b_{1u} (e_{2u}) active space orbitals are either entirely COT- or metal-based (i.e., ring π or f_δ), yields a total $n_f = 2 \times 0.216 = 0.432$ (Table 7). If we consider the atomic orbital contributions to the natural orbitals (NOs), and make the assumption that the metal- and COT-based basis functions are orthogonal to each other (which introduces an error in the metal orbital contribution to the NOs which we estimate to be less than 5%, based on the variation of NO normalization constants under the assumption that the basis used in these calculations is orthogonal), we can consider the π level (occupation 1.751) to be composed of 83.6% π and 16.4% f_δ, and the f_δ level to comprise 19.3% π and 80.7% f_δ. This significant covalency among the a_u and b_{1u} (e_{2u}) levels can be clearly seen in Figure 8. Using these contributions along with the natural occupation numbers of Table 7 yields a revised n_f of 0.92 ± 0.04. This n_f

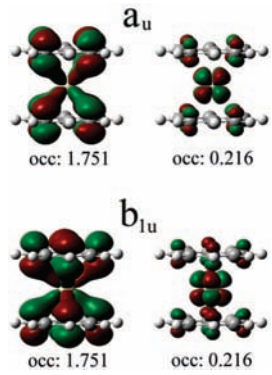

Figure 8. a_u and b_{1u} (e_{2u}) ground-state natural orbitals and occupations for $CeCOT_2$, illustrating the significant ring-metal covalency.

value is further discussed, and compared with both previous theory and experiment, in section 4.

Returning to Figure 6, we can see that, in comparison with $ThCOT_2$, the relative stabilization of the ground-state of $CeCOT_2$ is reduced from around 2.5 eV to c. 1.1 eV. Furthermore, whereas the lowest excited states of $ThCOT_2$ involve occupation of the d_σ level, in $CeCOT_2$ it is the f_σ level which is populated. In general, the low-lying $CeCOT_2$ excited states involve occupation of 4f levels, illustrating their stabilization relative to the 5d, by contrast to $ThCOT_2$. We can infer an energy level ordering for the metal levels of $E(f_\sigma) < E(f_\pi) < E(f_\delta)$, and from the lower relative energies of the *gerade* states compared with their *ungerade* counterparts for equivalent f level occupation, we can again conclude that the a_g and b_{1g} (e_{2g}) levels lie below the a_u and b_{1u} (e_{2u}) levels, as in $ThCOT_2$. This is to be expected because these levels are predominantly ligand based.

There are two experimentally observed excitations in the UV−vis spectrum of $CeCOT_2$, at 2.18 and 2.63 eV.[5] The lowest energy optically allowed transitions calculated here occur at 2.47 eV ($^1A_g \rightarrow {}^1B_{2u}/{}^1B_{3u}$; $\pi \rightarrow f_\pi$) and 2.93 eV ($^1A_g \rightarrow {}^1B_{1u}$; $\pi \rightarrow f_\delta$). Of these excitations, only the latter has a large oscillator strength, $f = 0.224$. Assuming that these excitations correspond to those determined experimentally, the discrepancy in each is approximately 0.3 eV, similar to that found for $ThCOT_2$.

3.2. The Effects of Spin−Orbit Coupling. ***(a) $ThCOT_2$.*** The 32 states calculated in part a of section 3.1 were used as a basis for spin−orbit coupling calculations, performed using the RASSI state-interaction method.[27] The inclusion of SOC has little effect on the ground-state electronic structure, although there are strong mixtures of the SOF states in the SOC excited states. The SOC-CASPT2 ground state is almost entirely (>99.99%) composed of its SOF counterpart, and the excited state that we suggest is seen experimentally in the UV−vis spectrum has an SOC energy of 2.49 eV, compared with 2.47 eV in the SOF calculations. The small variation in relative energy is produced by a 1% admixture of the lowest energy ^3A_u SOF state, which does nothing to render the excited-state optically accessible in the absence of vibronic coupling.

(b) $PaCOT_2$. By contrast to $ThCOT_2$, the effects of spin−orbit coupling in $PaCOT_2$ are expected to be pronounced, as has been shown in previous studies.[47,50] We were keen to establish that our computational method could handle such situations, and hence have used the 32 states calculated in part b of section 3.1 as a basis for SOC calculations. Figure 9 shows the lowest seven states in the absence and presence of spin orbit coupling, along with the SOF contributions to the SOC states, and the relative energies of these states are collected in Table 8, together with the results obtained by previous workers.

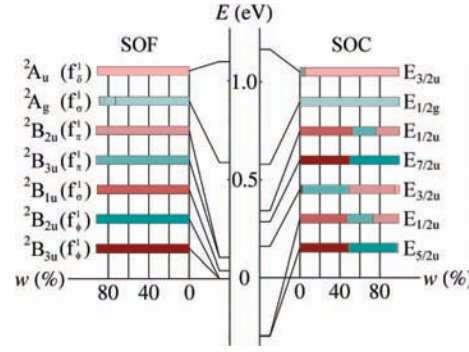

Figure 9. Comparison of the energy and composition of the seven lowest energy SOF and SOC states of $PaCOT_2$. The color-coding identifies the relative SOF contributions to the SOC states. Each of the SOC states is doubly degenerate. The D_{8h}* double point group labeling is inferred from ref 47.

TABLE 8: Comparison of the SOC State Energies (eV) of $PaCOT_2$ Obtained Here with Those of Previous Work

state	symmetry[a]	this work	Li and Bursten [b]	Chang et al. [c]
1	$E_{5/2u}$	0	0	0
2	$E_{1/2u}$	0.003	0.049	0.166
3	$E_{3/2u}$	0.459	0.369	0.477
4	$E_{7/2u}$	0.584	0.379	0.362
5	$E_{1/2u}$	0.642	0.541	0.569
6	$E_{1/2g}$	0.880	0.685	0.925
7	$E_{3/2u}$	1.467	1.122	1.222

[a] D_{8h}* symmetry assigned by Li and Bursten.[47] [b] DFT calculation using the PW91 exchange-correlation functional, using an optimized geometry with ring-metal separation of 1.975Å. Data from ref 47. [c] SOCI calculations at the experimental $UCOT_2$ geometry. Data from ref 41.

SOC has a significant effect on the energy spectrum of $PaCOT_2$. The SOC ground state lies 0.30 eV below its SOF counterpart, and is nearly degenerate ($\Delta E = 0.003$ eV) with the first SOC excited state (from which it has a significantly different orbital character). Given the very small energy difference between the ground and first excited SOC states, it would be inappropriate to assign the ground state without some measure of caution, although Table 8 shows that the ground state identified here is in agreement with that found in the two previous studies. Indeed, the general level of agreement between the present work and that reported previously is good, with states differing in relative energy by no more than ca. 0.2 eV.

Since the ground and first excited SOC states of $PaCOT_2$ are calculated to be so close in energy, we consider excitations from each of them. The transition with largest oscillator strength ($f = 3.3 \times 10^{-5}$) from the ground state occurs at 2.67 eV, in poor agreement with the value estimated from experiment, 3.4 eV.[49] A transition at 3.07 eV occurs from the first excited state and has a significantly larger oscillator strength ($f = 1.3 \times 10^{-4}$). The excited-state involved in this transition is dominated (82%) by $d_\sigma f_\phi$ occupation, and so the excitation appears to involve a $\pi \rightarrow d_\sigma$ transition, as well as an alteration in f level occupation. The ca. 0.3 eV difference in energy when compared with experiment is similar to that found in both $ThCOT_2$ and $CeCOT_2$.

(c) $CeCOT_2$. As with $ThCOT_2$, the effects of spin−orbit coupling in the ground state of this system are minimal; the SOC ground-state is 99.3% composed of its SOF counterpart. As seen in ref 10, excited SOC states are strong mixtures of the SOF states. As with the SOF calculations, we find only one strongly optically allowed transition ($f = 0.207$, vs $f = 0.224$

TABLE 9: Effect of Changing the Metal Basis Set on the Relative Energies (eV) of Selected States of $CeCOT_2$, $ThCOT_2$, and $PaCOT_2$

system	calculated states	ΔE (basis A)	ΔE (basis B)
$CeCOT_2$	^1A_g (ground state), $^1B_{2u}$	2.47	2.45
	^1A_g (ground state), $^1B_{3u}$	2.47	2.49
$ThCOT_2$	^1A_g (ground state), $^1B_{1u}$	2.47	2.37
$PaCOT_2$	$^2B_{1u}$, $^4B_{2g}$	2.36	2.35
	$^2B_{1u}$, $^2B_{2g}$	2.43	2.21

in the SOF calculations), occurring at 2.96 eV. The excited state is composed of 94.9% $^1B_{1u}$ (f_δ), with 2% contributions from the lowest energy $^3B_{2u}$ and $^3B_{3u}$ SOF states.

3.3. Effects of Basis Set Modifications. To assess the stability of our conclusions with respect to alterations of the basis sets, we have repeated a subset of the SOF calculations discussed above using the larger basis sets B and C (see Computational Details section for a description of these basis sets). Using basis B, we recalculated the energy differences between selected states, which differ in their formal metal orbital occupancy, and the results are collected in Table 9. For $CeCOT_2$ it can be seen that addition of g functions to the metal basis makes only 0.02 eV difference to the energy separation of the ^1A_g and $^1B_{2u}/^1B_{3u}$ states. We have assigned the first band in the experimental UV−vis spectrum to transition between these states − clearly the addition of g functions makes no difference to this interpretation. This is also the case for $ThCOT_2$, in which addition of g functions to the Th basis reduces the energy difference between the states assigned to the first optically allowed transition ($^1A_g \rightarrow {}^1B_{1u}$) by 0.1 eV (Table 9). We have repeated the latter calculation using basis C (which improves the C and H basis sets, as well as adding g functions to Th) and found that the $^1A_g/^1B_{1u}$ separation increased to 2.51 eV, very close to the value of 2.47 eV obtained using basis A. We therefore conclude that addition of g functions to the metal bases makes no substantive difference to the relative energies of the states found to be responsible for the lower energy experimentally observed transitions of $CeCOT_2$ and $ThCOT_2$.

The $^2B_{2u}/^2B_{3u}$ ground states of $PaCOT_2$ proved difficult to converge with basis B. The $^2B_{1u}$ state, however, which is almost degenerate with the $^2B_{2u}$ and $^2B_{3u}$ states, proved tractable, as did the optically accessible $^2B_{2g}$ state, although it required the orbitals of the $^4B_{2g}$ state to converge the lowest-energy $^2B_{2g}$ state with basis B. Table 9 shows that moving to basis B makes essentially no difference to the $^2B_{1u}/^4B_{2g}$ separation, though it does reduce that between the $^2B_{1u}$ and $^2B_{2g}$ states by 0.22 eV.

As discussed in part c of section 3.1, we have calculated, on the basis of the ground-state natural occupation numbers, an n_f value of 0.43, rising to 0.92 if we relax the restriction that the active space natural orbitals of a_u and b_{1u} (e_{2u}) symmetry are exclusively either ring π- or metal f_δ-based, that is that they have the covalent character illustrated in Figure 8. To probe the effect of basis set and active space size on these conclusions, we have repeated our two state average ^1A_g calculations with basis C and the (12,16) active space used in the partial geometry optimizations. The contribution of the d^0f^0 configuration to the ground state was found to be 53.8% (vs 58.1% from the smaller calculation, Figure 7), with the f^1 configuration contributing 26.0% (vs 23.4%). Importantly, when taking the corresponding variation in covalency in the NOs into account, the n_f value was also found to be little changed from that calculated using the smaller basis and active space (0.95 ± 0.04 vs 0.92 ± 0.04).

4. Discussion and Summary

Our results for $ThCOT_2$ and $PaCOT_2$ strongly suggest that the CASPT2 approach does an excellent job of describing the geometric and electronic structures. Metal−ring centroid distances are in very good agreement with experiment (and we note that applying the same methodology to $UCOT_2$ (which will be the subject of a future publication) yields a metal−ring distance of 1.926 Å, in comparison with the experimental value of 1.924 Å[2]). For $ThCOT_2$, we calculate excitation energies to lie within 0.3 eV of the experimental values, and the effects of spin−orbit coupling in $PaCOT_2$ are found to be comparable with those reported by previous workers.

For $CeCOT_2$, we reproduce the experimental metal−ring centroid distance to within 0.005 Å, locate the expected $^1A_{1g}$ ground-state, and calculate the first two electronic transitions of the UV−vis spectrum to within 0.3 eV. However, we disagree with previous workers as to the multiconfigurational nature of the ground state. Rather than the dominant Ce(III) configuration of Dolg et al., we find an almost 60% contribution from the Ce(IV) d^0f^0 configuration, with the f^1 configuration contributing only ca. 23%. We were rather surprised to discover such a discrepancy, although perhaps the differences between the two descriptions are not as large as might initially be assumed. As the electronic density is unchanged with respect to unitary transformations of the chosen basis (which can be defined here in terms of the configurational and molecular orbital coefficients), so an apparent difference in multiconfigurational character can in fact be due to such a rotation. This is particularly relevant in $CeCOT_2$, where the orbitals of most interest show significant covalency. In this case, large changes in configurational weights, if accompanied by variation in covalent character, can result in little or no variation in the overall density.

The ground state of ref 10 consists of 82.8% π^3f^1 and 17.2% π^4f^0, which, under the assumption of exclusively ring or f-based orbitals, yields $n_f = 0.83$. However, this good agreement with our value is seemingly at odds with our significantly differing description of the ground state in configurational terms. To probe this further, we have performed a series of state-averaged ^1A_g calculations, with the number of states included in the average ranging from 1 to 10, and the results are summarized in Figure 10. It can be seen that the ground-state NOOs are rather robust to variations in the size of the state average, as is the ground-state energy, which varies by no more than ca. 0.1 eV from the single-state energy at both the CASSCF and CASPT2 levels. By contrast, the variation in configurational admixture is remarkable, suggesting that description of the $CeCOT_2$ ground state in terms of specific contributing configurations of canonical orbitals is not robust. Rather, we prefer to rely on the NOOs as a quantitative diagnostic of multiconfigurational character, and the compositions and occupations of the NOs provide a reliable means for evaluating n_f. The stability of n_f with respect to state-average size (part a of Figure 10) allows us to confidently assert $n_f = 0.90 \pm 0.04$, the mean of the values obtained across the range of state averages.

Although neither the ground-state NOs nor their occupations are given in ref 10, our calculations indicate that the averaged (or pseudo-) natural orbitals become more localized as the size of the state-average is increased, for example the f character of the a_u/b_{1u} (e_{2u}) π level reduces from 16.4% in the single state calculation to only 2.9% in the 10-state average (by contrast, the ground-state NOs, and hence n_f, remain approximately constant). If the same is true in the calculations of ref 10, then an n_f value of 0.83 is only a small overestimate of the true calculated value.

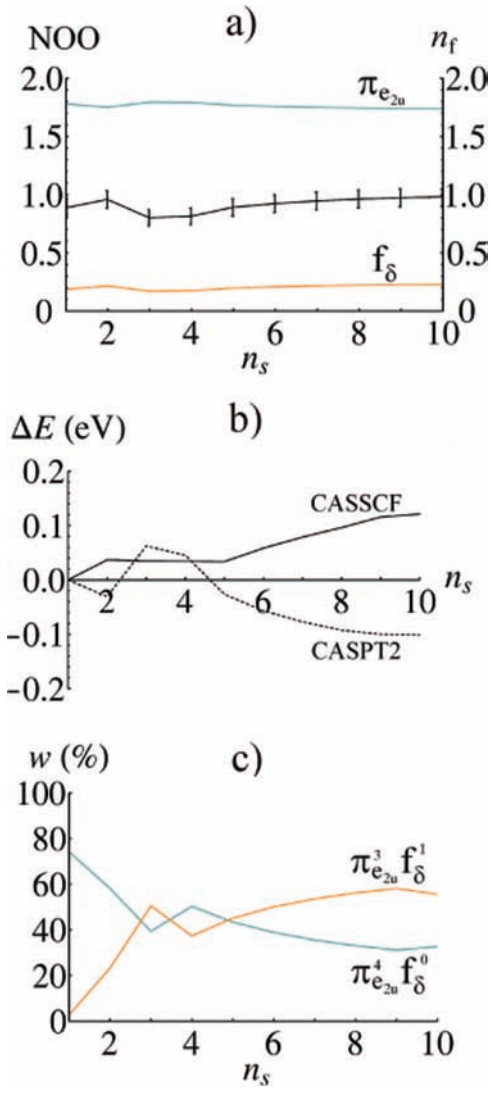

Figure 10. Variation of properties of the $CeCOT_2$ ^1A_g ground-state as the size of a state-averaged calculation (n_s) is increased. a) Variation of the ground-state natural orbital occupations (NOO) for the key a_u and b_{1u} (e_{2u}) orbitals, and corresponding n_f value. b) Variation of CASSCF and CASPT2 energies from those of the single state calculation. c) Variation of the weights of the π^4f^0 and π^3f^1 configurations. These configuration labels are only approximate because there is in fact significant covalency in the π and f levels (Figure 8).

Booth et al.[14] used Ce L_{III}-edge XANES to determine an n_f value of 0.89 ± 0.03, on the basis of a comparison of the spectrum of $CeCOT_2$ with those of Ce(III) and Ce(IV) standards. Notwithstanding the ambiguity that must surely arise in such experiments when "formally Ce(IV) systems generally are strongly mixed valent" and "the initial state of the Ce(IV) standard...is a superposition of states",[14] the agreement between the experimental and calculated values for n_f is remarkable; we all conclude that the Ce atom retains non-negligible f density.

So where does this leave the debate as to the oxidation state of Ce in $CeCOT_2$? Unfortunately, there is no simple answer to this question, as Figures 2 and 9 and Table 7 force us to abandon a simple orbital description based on a single configurational wave function. The entire concept of a formal oxidation state, which is weakened in the context of a multiconfigurational wave function, is not well defined for $CeCOT_2$. That said, we recognize that such statements are not entirely helpful to the experimental chemist. Our calculations indicate that there is appreciable Ce−COT covalency via the ring π/f_δ e_{2u} levels, and hence we are inclined to agree with refs 16 and 17 that $CeCOT_2$ is best described as Ce(IV) system in which transfer of electron density from ligand to metal through occupation of bonding orbitals allows measures of the effective oxidation state to be lower than the *formal* +4 value, and indeed closer to +3 in certain cases. If we make the simple distinction that a genuinely Ce(III) compound would be expected to have a metal-localized f electron, whereas a Ce(IV) compound would not, then cerocene fits better into the latter category, notwithstanding its significant f density.

We suggest that theoretical descriptions of the $CeCOT_2$ ground state are best given in terms of NOOs and not a configurational admixture. In any event, it is abundantly clear that f electron correlation is very important in $CeCOT_2$, by contrast to $ThCOT_2$. We look forward to probing the effects of such correlation as we move to the right in the 5f series, and these calculations will be the subject of future contributions.

Acknowledgment. We are grateful to the EPSRC for supporting this work via grants EP/C533054 and GR/S06233, and for the use of its National Service for Computational Chemistry Software (http://www.nsccs.ac.uk). We also thank UCL for a Teaching Assistantship to RC, and for computing resources via the Research Computing "Legion" cluster and associated services. We are also grateful to the reviewers for their helpful comments.

References and Notes

(1) Zalkin, A.; Raymond, K. N. *J. Am. Chem. Soc.* **1969**, *91*, 5667.
(2) Avdeef, A.; Zalkin, A.; Raymond, K. N.; Hodgson, K. O. *Inorg. Chem.* **1972**, *11*, 1083.
(3) Karraker, D. G.; Stone, J. A.; Jones, E. R.; Edelstein, N. *J. Am. Chem. Soc.* **1970**, *92*, 4841.
(4) Greco, A.; Cesca, S.; Bertolini, G. *J. Organomet. Chem.* **1976**, *113*, 321.
(5) Streitwieser, A.; Kinsley, S. A.; Rigsbee, J. T.; Fragala, I. L.; Ciliberto, E.; Rosch, N. *J. Am. Chem. Soc.* **1985**, *107*, 7786.
(6) Hodgson, K. O.; Raymond, K. N. *Inorg. Chem.* **1972**, *11*, 171.
(7) Raymond, K. N.; Eigenbrot, C. W. *Acc. Chem. Res.* **1980**, *13*, 276.
(8) Neumann, C. S.; Fulde, P. *Zeitschrift Fur Physik B-Condensed Matter* **1989**, *74*, 277.
(9) Dolg, M.; Fulde, P.; Kuechle, W.; Neumann, C. S.; Stoll, H. *J. Chem. Phys.* **1991**, *94*, 3011.
(10) Dolg, M.; Fulde, P.; Stoll, H.; Preuss, H.; Chang, A.; Pitzer, R. M. *Chem. Phys.* **1995**, *195*, 71.
(11) Liu, W. J.; Dolg, M.; Fulde, P. *J. Chem. Phys.* **1997**, *107*, 3584.
(12) Liu, W. J.; Dolg, M.; Fulde, P. *Inorg. Chem.* **1998**, *37*, 1067.
(13) Edelstein, N. M.; Allen, P. G.; Bucher, J. J.; Shuh, D. K.; Sofield, C. D.; Kaltsoyannis, N.; Maunder, G. H.; Russo, M. R.; Sella, A. *J. Am. Chem. Soc.* **1996**, *118*, 13115.
(14) Booth, C. H.; Walter, M. D.; Daniel, M.; Lukens, W. W.; Andersen, R. A. *Phys. Rev. Lett.* **2005**, *95*, 267202.
(15) Amberger, H. D.; Reddmann, H.; Edelmann, F. T. *J. Organomet. Chem.* **2005**, *690*, 2238.
(16) Streitwieser, A.; Kinsley, S. A.; Jenson, C. H.; Rigsbee, J. T. *Organometallics* **2004**, *23*, 5169.
(17) Balazs, G.; Cloke, F. G. N.; Green, J. C.; Harker, R. M.; Harrison, A.; Hitchcock, P. B.; Jardine, C. N.; Walton, R. *Organometallics* **2007**, *26*, 3111.
(18) Ashley, A.; Balazs, G.; Cowley, A.; Green, J.; Booth, C. H.; O'Hare, D. *Chem. Commun.* **2007**, 1515.
(19) Riseborough, P. S. *Adv. Phys.* **2000**, *49*, 257.
(20) Kotani, A.; Mizuta, H.; Jo, T.; Parlebas, J. C. *Solid State Commun.* **1985**, *53*, 805.
(21) Gilbert, A.; Vidhyadhiraja, N. S.; Logan, D. E. *J. Phys.: Condens. Matter* **2007**, *19*, 106220.
(22) Kaltsoyannis, N.; Scott, P. *The f elements*; Oxford University Press: Oxford, 1999.
(23) Roos, B. O.; Taylor, P. R. *Chem. Phys.* **1980**, *48*, 157.
(24) Roos, B. O. *Advances in Chemical Physics; Ab Initio Methods in Quantum Chemistry - II*; Lawley, K. P., Ed.; John Wiley & Sons Ltd.: Chichester, 1987.
(25) Douglas, M.; Kroll, N. M. *Ann. Phys.* **1974**, *82*, 89.
(26) Andersson, K.; Malmqvist, P. A.; Roos, B. O.; Sadlej, A. J.; Wolinski, K. *J. Phys. Chem.* **1990**, *94*, 5483.

(27) Malmqvist, P. A.; Roos, B. O.; Schimmelpfennig, B. *Chem. Phys. Lett.* **2002**, *357*, 230.
(28) Karlstrom, G.; Lindh, R.; Malmqvist, P. A.; Roos, B. O.; Ryde, U.; Veryazov, V.; Widmark, P. O.; Cossi, M.; Schimmelpfennig, B.; Neogrady, P.; Seijo, L. *Comput. Mater. Sci.* **2003**, *28*, 222.
(29) Roos, B. O. Unpublished results.
(30) Hunt, W. J.; Goddard, W. A. *Chem. Phys. Lett.* **1969**, *3*, 414.
(31) *MOLCAS Version 6.4 User's Manual*, Lund University, 2006, 129.
(32) Lowdin, P. O. *Phys. Rev.* **1955**, *97*, 1474.
(33) Frisch, M. J.; Trucks, G. W.; Schlegel, H. B.; Scuseria, G. E.; Robb, M. A.; Cheeseman, J. R.; Montgomery, J., J. A.; Vreven, T.; Kudin, K. N.; Burant, J. C.; Millam, J. M.; Iyengar, S. S.; Tomasi, J.; Barone, V.; Mennucci, B.; Cossi, M.; Scalmani, G.; Rega, N.; Petersson, G. A.; Nakatsuji, H.; Hada, M.; Ehara, M.; Toyota, K.; Fukuda, R.; Hasegawa, J.; Ishida, M.; Nakajima, T.; Honda, Y.; Kitao, O.; Nakai, H.; Klene, M.; Li, X.; Knox, J. E.; Hratchian, H. P.; Cross, J. B.; Bakken, V.; Adamo, C.; Jaramillo, J.; Gomperts, R.; Stratmann, R. E.; Yazyev, O.; Austin, A. J.; Cammi, R.; Pomelli, C.; Ochterski, J. W.; Ayala, P. Y.; Morokuma, K.; Voth, G. A.; Salvador, P.; Dannenberg, J. J.; Zakrzewski, V. G.; Dapprich, S.; Daniels, A. D.; Strain, M. C.; Farkas, O.; Malick, D. K.; Rabuck, A. D.; Raghavachari, K.; Foresman, J. B.; Ortiz, J. V.; Cui, Q.; Baboul, A. G.; Clifford, S.; Cioslowski, J.; Stefanov, B. B.; Liu, G.; Liashenko, A.; Piskorz, P.; Komaromi, I.; Martin, R. L.; Fox, D. J.; Keith, T.; Al-Laham, M. A.; Peng, C. Y.; Nanayakkara, A.; Challacombe, M.; Gill, P. M. W.; Johnson, B.; Chen, W.; Wong, M. W.; Gonzalez, C.; Pople, J. A. *Gaussian 03*, revision D.01; Gaussian, Inc.: Wallingford, CT, 2004.
(34) Becke, A. D. *J. Chem. Phys.* **1993**, *98*, 1372.
(35) Becke, A. D. *Phys. Rev. A* **1988**, *38*, 3098.
(36) Lee, C. T.; Yang, W. T.; Parr, R. G. *Phys. Rev. B* **1988**, *37*, 785.
(37) Dunning, T. H. *J. Chem. Phys.* **1989**, *90*, 1007.
(38) Kuechle, W.; Dolg, M.; Stoll, H.; Preuss, H. *J. Chem. Phys.* **1994**, *100*, 7535.
(39) Cao, X. Y.; Dolg, M.; Stoll, H. *J. Chem. Phys.* **2003**, *118*, 487.
(40) Chang, A. H. H.; Pitzer, R. M. *J. Am. Chem. Soc.* **1989**, *111*, 2500.
(41) Chang, A. H. H.; Zhao, K.; Ermler, W. C.; Pitzer, R. M. *J. Alloys Compd.* **1994**, *213/214*, 191.
(42) Schmidt, M. W.; Gordon, M. S. *Annu. Rev. Phys. Chem.* **1998**, *49*, 233.
(43) Kot, W. K.; Shalimoff, G. V.; Edelstein, N. M.; Edelman, M. A.; Lappert, M. F. *J. Am. Chem. Soc.* **1988**, *110*, 986.
(44) Kaltsoyannis, N.; Bursten, B. E. *J. Organomet. Chem.* **1997**, *528*, 19.
(45) Levanda, C.; Streitwieser, A. *Inorg. Chem.* **1981**, *20*, 656.
(46) Rösch, N.; Streitwieser, A. *J. Am. Chem. Soc.* **1983**, *105*, 7237.
(47) Li, J.; Bursten, B. E. *J. Am. Chem. Soc.* **1998**, *120*, 11456.
(48) Perdew, J. P.; Chevary, J. A.; Vosko, S. H.; Jackson, K. A.; Pederson, M. R.; Singh, D. J.; Fiolhais, C. *Phys. Rev. B* **1992**, *46*, 6671.
(49) Solar, J. P.; Burghard, H. P. G.; Banks, R. H.; Streitwieser, A. J.; Brown, D. *Inorg. Chem.* **1980**, *19*, 2186.
(50) Zhao, K., Ph.D. Thesis, The Ohio State University, 1996.

JP807804W